Investigation of focal ratio degradation in optical fibres for astronomical instrumentation

Lisa Crause[a*], Matthew Bershady[b], David Buckley[a]
[a]South African Astronomical Observatory, P. O. Box 9, Observatory 7935, South Africa;
[b]University of Wisconsin, Department of Astronomy, 475 N Charter St., Madison, WI, USA 53706

ABSTRACT

A differential method was used to investigate the focal ratio degradation (FRD) exhibited by, and throughput of, a selection of current-generation optical fibres. These fibres were tested to establish which would be best suited to feed the High Resolution Spectrograph being built for the Southern African Large Telescope (SALT), as well as for future instruments on WIYN and SALT. The double re-imaging system of Bershady et al. (2004) was substantially modified to improve image quality and measurement efficiency, and to permit a direct FRD-measurement in the far-field. The re-imaging method compares the beam profile produced by light which passes through a fibre to that which does not. Broad and intermediate band-pass filters were used between 400-800 nm to test for wavelength dependence in the observed FRD over a wide range in beam-speeds. Our results continue to be at odds with a mico-bend model for FRD. We conclude that the new Polymicro FBP fibre is the most suitable product for broadband applications.

Keywords: multi-mode fibres, focal ratio degradation

1. INTRODUCTION

1.1 Goals

Fibre optics for astronomy offer a relatively efficient but very cost-effective way to direct and reformat the telescope to spectrograph image planes. The principle drawback to fibre use has been their introduction of entropy, in the form of FRD, and signal attenuation, particularly in the blue. However, broad-band multi-mode fibres, such as Polymicro's FIP-STU product, and more recently their FBP series, minimize transmission losses – at least between 400 and 1700 nm. Combined with trends of increasing instrument size and cost, there is a revived interest in fibre optic fed instruments, even in the near-infrared[1]. This is particularly true on HET-style telescopes, such as SALT, where the weight-bearing capacity at prime focus is limited. With that in mind, we have returned to the question of what causes FRD, its quantification, and what can be done to minimize it in preparation and handling. At the same time, we are keenly aware that the most cited model for FRD[2], which invokes micro-bends, predicts a wavelength-dependence to FRD (increasing at longer wavelengths) which is either not observed or observed at a much-decreased amplitude relative to model expectations. This mismatch between observation and theory is unsettling. The laboratory setting offers a controlled opportunity to revisit the observational picture, improve upon our understanding of the FRD phenomenon, and learn how it can be reduced.

1.2 Approach

Our approach has been to develop two complementary methods for measuring FRD, along the lines laid out by Carrasco and Parry[3]. The first is to create an optical system which permits a differential measurement of both throughput and FRD. In this case, an input beam is formed which can mimic that created by a telescope. It is sampled both directly (without fibre optics), and again after passing through fibre optics such that both the beam degradation in profile and

* lisa@saao.ac.za

Ground-based and Airborne Instrumentation for Astronomy II, edited by Ian S. McLean, Mark M. Casali,
Proc. of SPIE Vol. 7014, 70146C, (2008) · 0277-786X/08/$18 · doi: 10.1117/12.791041

amplitude can be determined with respect to the direct reference. This differential approach has many merits both in terms of mimicking real astronomical application and analysis simplicity. However, the measurements themselves can be laborious, particularly if multiple beam-speeds, filters, or input beam-profiles are desired. We refer to this as the formed-beam method.

A more elegant approach is to feed fibres with collimated light, e.g., a laser, and observe the output ring of light (angle and width) as a function of input angle. In principle, such measurements can be related to an FRD model, and therefore the FRD for any arbitrary input beam can be simulated based on relatively few measurements. The further advantage of this approach is that both the ring angle (deviation from input angle) and width (spread of angles) can be measured; these quantities cannot be disentangled from the formed-beam approach. Disadvantages of this collimated-beam approach include the inability to make a throughput measurement in a well-controlled manner, and also that it is not differential, (it relies on the quality of the collimation of the input beam).

1.3 Scope of present work

Here we describe the initial step of building, aligning, and calibrating the formed-beam measuring apparatus, along with the first measurements made on 9 different types of fibre from two vendors. The measuring engine is designed to allow for accurate and precise determinations of FRD as a function of input beam-speed, wavelength, spot-size and near-field input location at the 10-micron level of the fibre face. Of specific interest is the evaluation of several fibre brands for the High Resolution Spectrograph under construction for SALT at the Durham University Centre for Advanced Instrumentation, other IFUs for the WIYN 3.5m Telescope Bench Spectrograph, and possible future instruments on these and other telescopes. We describe results which led to a positive re-assessment of the blue-performance of the science-active SparsePak IFU on the WIYN 3.5m telescope, identify the most promising fibres for upcoming and future instruments, and compare metrics for assessment of fibre performance.

2. FORMED-BEAM APPARATUS

2.1 FRD and throughput measuring engine

The re-imaging system of Bershady et al. (2004) was adapted to yield a collimated beam and this far-field illumination pattern is then imaged in two modes (the direct mode which serves as a reference and the actual fibre testing mode) to obtain a differential measurement. Although we used an open aperture, the test apparatus would easily allow for the addition of an obscured beam (e.g, a tracker + payload or a classical secondary).

This description of the apparatus follows the schematic in Fig. 1. A halogen light source is connected by a coherent fibre bundle (F1) to a unit housing a filter (F), diffuser (D) and pinhole (PH). Light diverging from the pinhole is captured by the first lens (L1) which collimates the beam before it passes through an iris which sets the speed of the input beam. The second lens (L2) is a camera which brings the light to an intermediate focus. All of these components, as well as the mount for the fibre output, are located on a large translation stage that can be moved perpendicular to the beam, as shown in Fig. 1. In the direct mode, light from the intermediate focus then enters a second collimator (L3) and the beam is imaged by the CCD camera. In the fibre mode, the translation stage is set such that the L2 focus falls on the fibre input face and the output face is then aligned so as to feed L3 which produces the fibre beam to be imaged.

A single measurement – whether part of a filter sequence (R, I, y, b, v), or a beam-speed sequence (input f-ratios of 3.0, 4.2, 6.3, 10.0 and 13.7) – consists of a fibre mode image, followed by a direct image and then a second fibre mode image. Ideally the beam switching should set precisely for each mode, but in practice the process involves manually shifting the translation stage to fiducial marks and then tweaking the position based on the location of either the direct beam on the CCD frame, or the actual spot on the fibre face (viewed via M1) in the case of the fibre mode. The latter is problematic for I-band measurements as the spot is not visible by eye and so for the second fibre image in a set, one has to peak-up the stage position based on the counts in the CCD frame. Despite this complication for the I-band, agreement between the two fibre mode images was always extremely good and the results were typically indistinguishable.

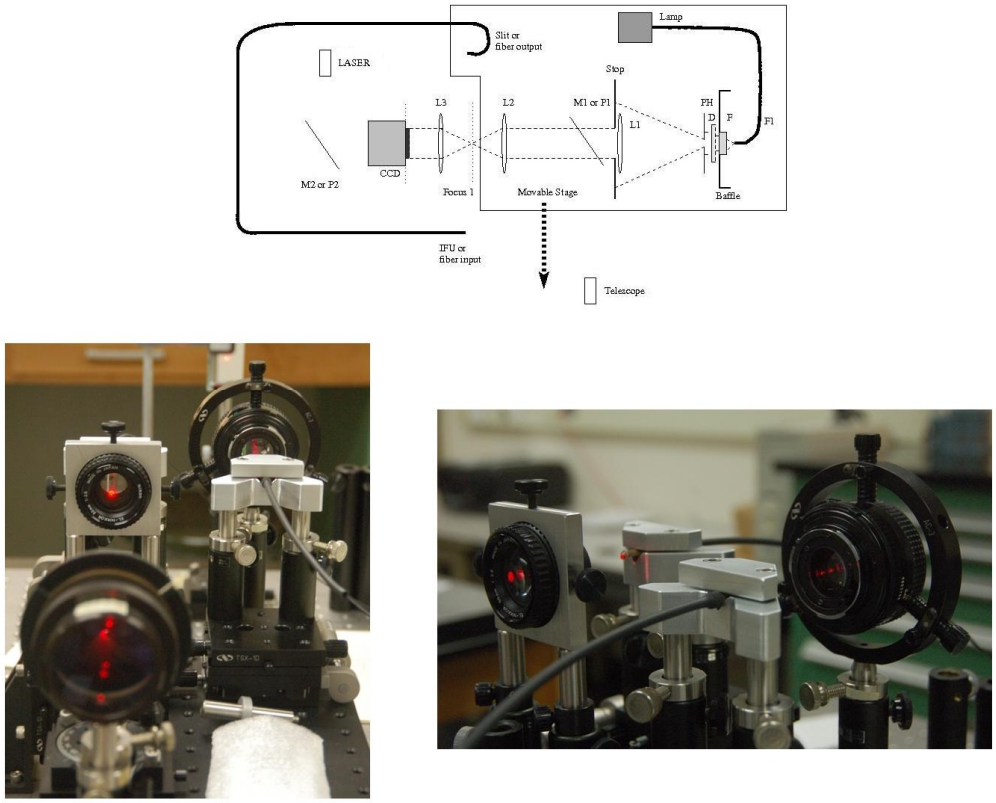

Fig. 1: Schematic of the FRD and throughput measuring engine and photographs showing key elements of the re-imaging system. The left-hand photo is looking along the light path with L1 in the foreground, followed by the iris used to set the input beam-speed. Next, the Nikon 50 mm f/2.8 (L2) focuses light from the pinhole onto the input face of the fibre and the fibre exit feeds the 50 mm f/1.7 Minolta lens (L3) that produces the collimated beam to be imaged by the CCD (not shown). Note the ferrule holders mounted on two posts to avoid telecentricity deviations.

The initial set of lenses[5] consisted of three achromatic doublets, resulting in a system that exhibited severe spherical aberration. Simple Zemax models indicated that the effect could be significantly reduced with a longer focal length doublet at L1 and so we adopted a 250 mm achromat. Furthermore, replacing the L2 and L3 doublets with commercial camera lenses (available in the lab) proved extremely effective in removing the remaining aberrations. At first we worked with the f/1.7 lens at L2, but later moved it to L3 to take advantage of the larger aperture, since the beam emerging from a fibre is always faster than the injected beam. The final system thus employed a 250 mm achromat for L1, a 50 mm Nikon f/2.8 lens for L2 and a 50 mm f/1.7 Minolta lens for L3 – see the photographs in Fig. 1.

The system is extremely sensitive to alignment and various components need to be focused, namely the two collimators and the two fibre ends. Overall alignment of the optics was achieved by removing the CCD and injecting a laser (from the upper left in Fig. 1) along the optical path in the direct imaging mode. A fold flat mounted on a precision rotation stage at M2 was set perpendicular to the laser by adjusting it until the beam reflected on itself and the mirror could then be rotated 45° to direct the laser towards the pinhole. Additional irises were placed along the path and stopped down as much as possible to check the relative alignment of the translation stage and the rest of the optical bench. The lenses could then be adjusted in height, yaw and perpendicular to the beam until the series of spots on each surface lined up perfectly en route to the pinhole. Three-point ring mounts for holding lenses (L3 in Fig. 1) proved extremely tedious to align properly, and are being replaced with custom mounts (L2 in Fig. 1).

Once aligned, the lenses (mounted on micrometer stages) could be focused using an auto-collimation process. For L1, a mirror placed in front of L2 reflects light back to the pinhole while a pellicle at position P1 in Fig. 1 allows one to view the pinhole and the reflected spot with a small telescope. The L1 focus is adjusted until the spot sizes match. The same technique is used for L3, by placing the mirror at M2 and the pellicle between L3 and M2. The L1 and L3 focus settings then remain fixed and all subsequent focus changes are made in the fibre mode, by adjusting the fibre input and output faces. The L2 position does not need to be set carefully as the fibre ends get adjusted to reach the location of the intermediate focus. With the system in the fibre mode, the spot on the input face is viewed via the pellicle/telescope combination fed from M1 – the position of the fibre end is adjusted in x and y until the spot is centred on the face and in z until best focus is achieved. Focusing the output face is a similar process, but requires a collimated beam to be fed into the back of L3 and focused to produce a spot on the fibre face (since light from the pinhole illuminates the whole output face, not simply a spot as is the case on the input side). This is achieved by passing the laser through a beam expander and neutral density film before reaching L3. The heavily attenuated laser spot can then be viewed via the pellicle between M2 and L3 and the z position of the output face adjusted to produce a sharp spot on the exit face. Provided nothing else is disrupted, further focusing is only necessary whenever a new fibre is installed for testing.

An important refinement of the Bershady et al. system was redesigning the ferrule holders to be mounted on two posts. This eliminates a troublesome degree of freedom which introduces non-telecentric effects that add to the measured FRD. To our chagrin, however, late in the measurement process we discovered two wedge-angles produced by the combination of angle-brackets and stages that make up the adjustable platform for mounting the input face of the fibre. These angles were estimated to be 0.33° in one axis and 0.24° in another, which in quadrature amounts to 0.41°. Referring to Bershady et al. (2004) fig. 12, this amount of wedge introduces a beam-speed increase from f/4.2 to roughly f/4.1, but would degrade an f/13.7 input beam to about f/12.6. However, one set of measurements was repeated after the 0.33° wedge was removed and we found essentially no difference between the two sets of results – see Section 3.4 and Fig. 7. We thus conclude that our measurements were not significantly compromised by the misalignment as the system is not particularly sensitive to such small telecentricity deviations.

Although the high quality camera lenses produce good image quality, our system could still be improved in a number of ways. The translation stage for switching between direct and fibre beams is cumbersome and so we investigated using a set of mirrors to steer the beam – as suggested in fig. 4 of Ramsey[3]. Hardware limitations prevented us implementing the mirror system, but we would recommend this approach. Filter changes are also problematic as access to the filter is achieved by removing the unit holding the diffuser and pinhole. Replacing the unit does not always set the pinhole back reliably, thus degrading the beam quality. A better design would have the filters mounted in a sliding mechanism which would allow filter changes without disruption of the pinhole. Finally, the system is quite sensitive to stray light sources within the lab. Most of these were eliminated or carefully baffled to keep the background flat, but stray light can still be a problem for the longer exposures sometimes needed for the I and v (near ultra-violet) filters.

2.2 Characterizing the direct system: intermediate focus and collimated beam profile

To test for a wavelength dependence to the L1 focus, we obtained a sequence of images of the initial collimated beam – at the best focus found with the auto-collimation technique described in Section 2.1 – through the various filters (and in white light) with the CCD fed by M1. As the radii at given EE values were essentially flat across the full wavelength range, we elected not to attempt to refocus L1 for each filter. Given the quality of commercial camera lenses relative to achromats, we did not expect to find a wavelength dependence in L2 or L3 either and this was subsequently confirmed when comparing the filtered spots observed on the fibre input face, as well as the beam sizes measured in the direct images.

A CCD camera with 9 micron pixels was placed at the intermediate focus to evaluate the image quality of the collimator-camera system (a 250 mm achromat at L1 and a 50 mm f/1.7 Minolta lens at L2, resulting in a demagnification of 0.2). The combination produced excellent image quality with EE95 being less than 50 microns for a 10 micron pinhole. Later rearrangements placed the Minolta lens at L3 and a 50 mm f/2.8 Nikon lens at L2, but this did not appear to affect the image quality.

We were surprised by the amount of structure seen in the direct beam, particularly the diffraction patterns in the left-hand image in Fig. 2. These features are pronounced when working with 10 and 100 micron pinholes, but are washed out in images obtained with the 600 and 1000 micron pinholes used in the actual fibre measurements. Dark, patchy features seen in direct beam images (not shown in Fig. 2) were eliminated by replacing the ground glass diffuser with an

opal diffuser. The deviation of the direct beam from the ideal top-hat function (see the brightness profiles in Fig.2) is not considered problematic as all the measurements are differential.

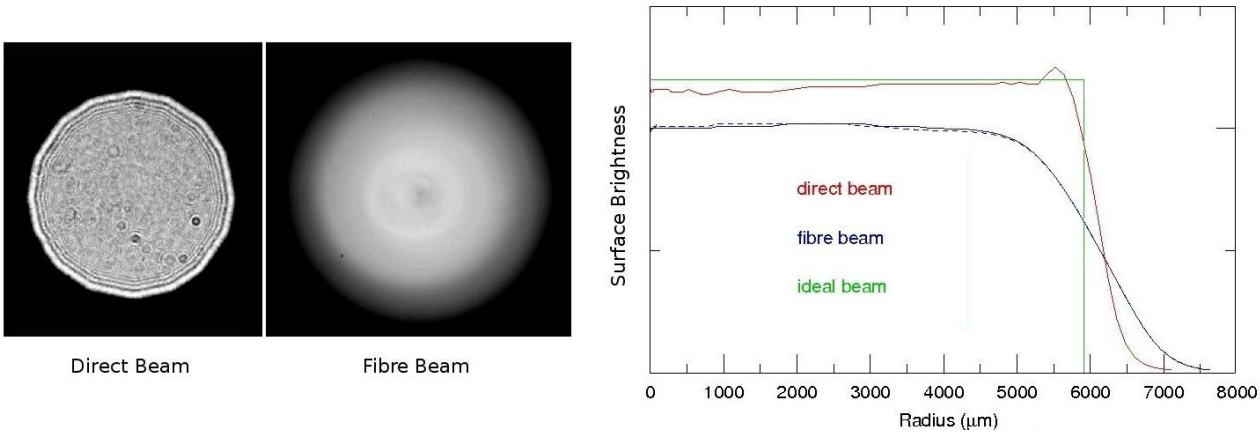

Fig. 2: Typical far-field images of the direct and fibre beams obtained with a 10 micron pinhole, as well as the resulting beam profiles, with an ideal f/4.2 beam (top-hat function) shown for comparison. The dashed blue curve is from the second fibre beam image in the set and shows good agreement with the first.

3. FIBRE MEASUREMENTS

3.1 The fibres and the tests

A selection of optical fibres from two major vendors, Polymicro and CeramOptec, were obtained and prepared for testing to determine their throughput and FRD properties as a function of wavelength (see Table 1 for filter information) and input beam-speed. These fibres have a variety of spectral responses, diameters ranging from 200 – 600 microns and lengths between 15 and 35 m (see Table 2 for details), making for an interesting comparative study.

Other than the SparsePak Reference cable which was also measured with Johnson B and V filters, all fibres were tested with Johnson I and R filters and Stromgren y, b and v filters. These wavelength measurements were made for an input beam-speed of f/4.2, corresponding to the output f-ratio of SALT. Four fibres were also tested in the R-band at different input beam-speeds, including the WIYN Bench Spectrograph's f/6.3, the WIYN Cassegrain's f/13.7 and arbitrarily chosen f/3.0 and f/10.0 to supplement the range. Filter sequences at f/13.7 were also obtained for the SparsePak Reference fibre and the Polymicro FBP 600 micron fibre as FRD is more pronounced for slower beams, making this regime more sensitive to possible wavelength dependent effects.

Table 1: Johnson broad-band and Stromgren narrow-band filter central wavelengths and FWHM.

Filter	**U**	**B**	**V**	**R**	**I**	**u**	**v**	**b**	**y**
Central wavelength λ_c (nm)	360	440	550	640	790	353.7	410.3	473.0	550.7
$d\lambda/\lambda$	0.15	0.22	0.16	0.23	0.19	0.079	0.039	0.041	0.045

Table 2: Throughput and FRD measurements for the selection of fibres tested. We note that the fibre with the best end preparation (the SparsePak reference cable) performs significantly better than all the other samples. Despite these termination issues, we conclude that the new Polymicro FBP fibre is superior, particularly in comparison with the CeramOptec UV range that performs poorly in the blue. See Sections 3.2 for an explanation of the beam correction process.

Manufacturer	Fibre Type	Core/Clad/Buffer diameters (μm)	Length (m)	R throughput at f/4.2	I/v throughput ratio	Uncorrected EE95 output for f/4.2 input	Corrected EE95 output for f/4.2 input
Polymicro	FIP-STU?	500/550/600 *	25.4	0.89	1.13	3.89	3.99
Polymicro	FIP-STU	200/220/240	35.0	0.85	1.09	3.81	3.94
Polymicro	FVP	400/440/480	35.0	0.75	1.15	3.67	3.77
Polymicro	FBP	300/330/370	30.0	0.70	1.08	3.24	3.24
Polymicro	FBP	400/440/480	30.0	0.84	1.05	3.39	3.46
Polymicro	FBP	600/660/710	15.0	0.80	1.03	3.56	3.65
CeramOptec	UV	200/220/245	35.0	0.81	1.13	3.39	3.48
CeramOptec	UV	400/440/470	35.0	0.77	1.17	3.09	3.13
CeramOptec	UV	600/660/710	35.0	0.84	1.16	3.67	3.75

* SparsePak Reference fibre

3.2 General analysis

The two fibre parameters we derive from the images shown in Fig. 2 are related to the profile shape (FRD) and the amplitude (throughput). To do this, we integrate the cross-sectional intensity distribution of the beam (the light profile) to generate a curve of growth for the encircled energy. We then define quantities such as EE50, EE80, EE90 and EE95 based on this curve of growth. We make a correction to the fibre beam profile based on the departure of the direct beam profile from an ideal beam of constant cross-sectional surface-brightness. The correction is made in quadrature to each radius at a given encircled energy; by definition, this correction, when applied to the direct beam, yields the ideal beam profile. This is demonstrated in Fig. 3.

At a given input f-ratio there are a number of ways to define the FRD. We explore input f-ratio vs output f-ratio and the trends of throughput with input f-ratio in Section 3.7 below. Likewise, both FRD and throughput can be defined at any given EE. While throughput is independent of this choice, FRD is not since in general the fibre-aberrated profile (a smeared-out version of the ideal top-hat function) has a long tail to high beam-speeds. A common practice in the literature is to adopt EE95 for FRD (as we tabulate), but the trend with EE, which we show in Fig. 4, is perhaps more instructive as a means to evaluate performance design-trades in fibre-fed instruments. In the SparsePak Reference fibre case illustrated, we see that more than 70% of the exit-beam is contained within the input beam f-number, but that the optics handling the output-beam would have to be 8% faster to contain 95% of the exit beam.

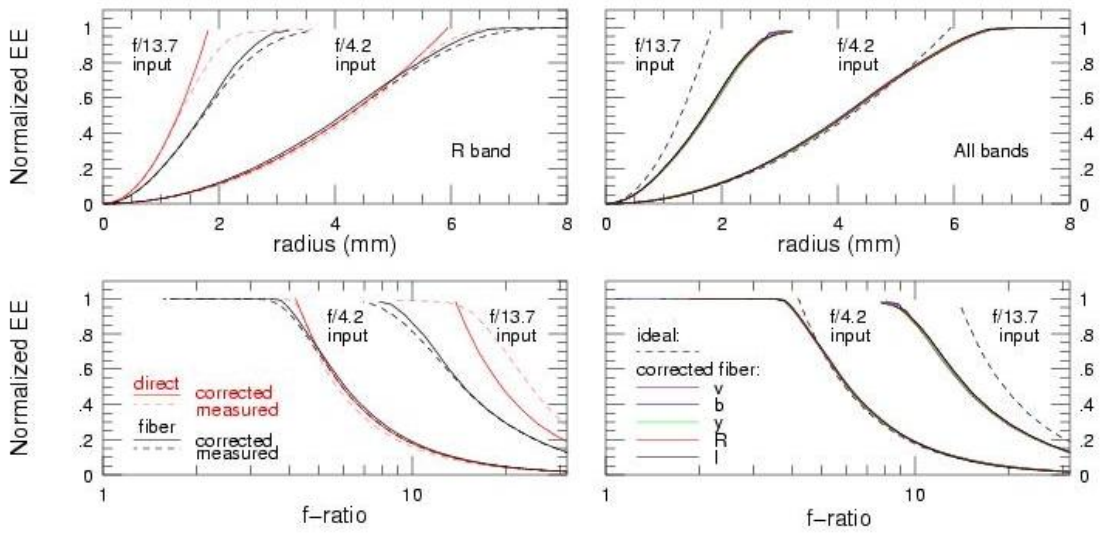

Fig. 3: FRD measurements in the form of curves of growth (plotted vs radius and f-ratio in the upper and lower panels respectively) for the SparsePak Reference fibre with input beam-speeds of f/4.2 and f/13.7. Solid lines indicate corrected data in all panels while the dashed curves correspond to measured data in the left-hand column (R-band only) and ideal beams in the right-hand column (which includes all bands: I, R, y, b and v). See Section 3.2 for details of the correction process.

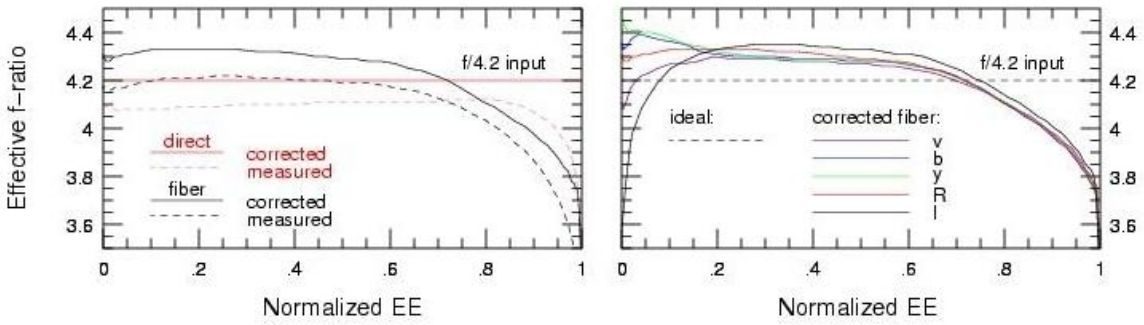

Fig. 4: Our preferred way of presenting FRD measurements: the effective f-ratio as a function of fractional encircled energy. The left panel shows R-band data, both measured and corrected, while the right panel shows the corrected data for all the bands used to measure the SparsePak Reference fibre (with an f/4.2 input beam) – note the good agreement over the range of wavelengths tested.

3.3 Throughput results

Fig. 5 shows the absolute throughput of the SparsePak Reference fibre on the left and the normalized curves for all the other fibres on the right. See figure caption for key to line colours and types. This normalization with respect to the R-band throughput of the SparsePak Reference cable was done to highlight the differential behaviour of the various fibres with wavelength. This approach was chosen in an attempt to take into account the degraded throughput due to fibre end-effects in some fibres (see section 3.6), which we assume to be only weakly dependent on wavelength. The CeramOptec fibres are particularly poor in the UV, clearly unsuitable for use on SALT which is optimized for good blue performance. The FVP 400 fibre also fares badly in the blue, while the SparsePak Reference fibre and the FIP-STU 200 are similar to one another and superior in the blue. However, the response curves for the new Polymicro FBP range are flatter than all the others, making them the most appropriate choice for broadband applications.

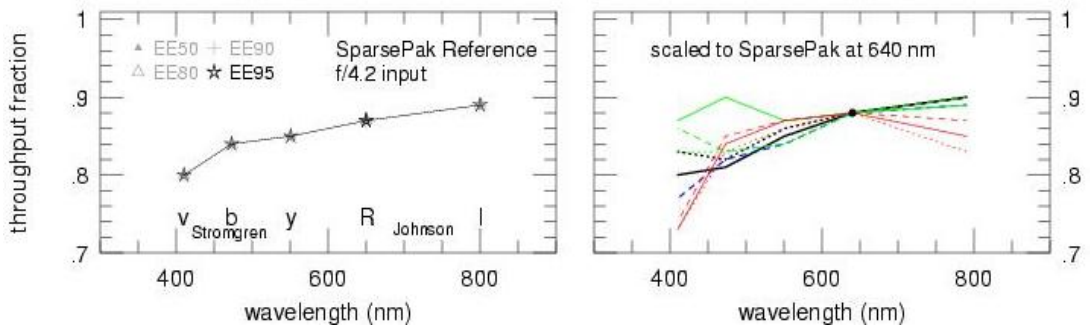

Fig. 5: The absolute throughput vs wavelength for the SparsePak Reference fibre is shown in the panel on the left. On the right we have normalized all the other fibres tested relative to the SparsePak R-band (640 nm) throughput. The lines are as follows: black (SparsePak Reference and Polymicro FIP-STU), blue (Polymicro FVP), green (Polymicro FBP) and red (CeramOptec UV). Line types are: dotted (200-300 micron), dashed (400 micron), solid (500-600 micron).

3.4 SparsePak Reference Cable performance

During manufacture of the SparsePak IFU for WIYN[5,6], a 25.4m strand was prepared and carefully spooled, terminated, polished, and set aside from the IFU as a reference cable. The fibre purchased was supposedly FIP ultra-low OH^- fused silica. At the time (March 2001), FRD and throughput measurements were made on the reference cable as well as the IFU in the four broad bands (Johnson B, V, R and I), with the puzzling result that the B-band throughput measurements were higher than expected, despite excellent agreement between vendor-supplied transmission curves (including surface reflection losses) and measurements in the V, R, and I bands. This result was then attributed to the broad band-pass of the B filter combined with rapid fall-off in the fibre transmission and the red color of the line-lamp (see [4] for further discussion), all of which, it was surmised, led to an effective wavelength redder than the mean wavelength of the filter transmission curve.

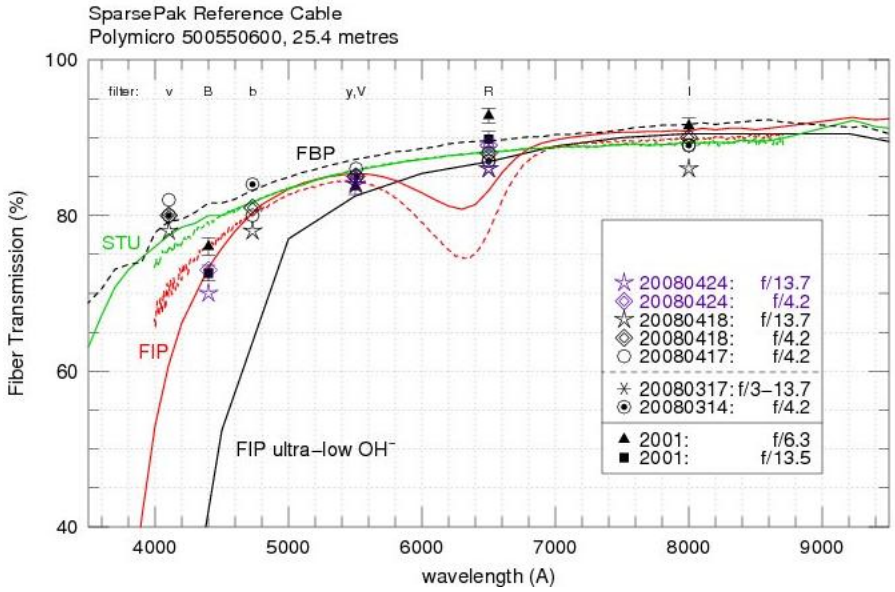

Fig. 6: SparsePak result: the vendor transmission curve for FIP from 2001 is black and the current vendor curve for the same product is shown in red. While the B-band data is consistent with the more modern FIP curve, there is no dip in the R-band. Overall, the SparsePak data, when considering the narrow Stromgren bands in the blue, best match the vendor predictions for FIP-STU or FBP. We surmise that the SparsePak project received FIP-STU fibre, unbeknownst, and therefore should perform well down to 400 nm, as recent observations on WIYN indicate[7].

Re-measurement of this fibre, in the same physical state in 2008 shows the same relative throughput performance in the BVR bands, but different behaviour in the blue when we use the narrow Stromgren b and v filters. We therefore revise our interpretation as still a band-pass effect, but one which is due to poor performance at the blue end of the broad B-band filter (which has a 50% power-point at 378 nm) but with an overall transmission curve that is better in the the blue than the FIP fibre. As illustrated in Fig. 6, the SparsePak Reference fibre shows transmission very similar to FIP-STU, and quite comparable to FBP in this wavelength range. This bodes well for blue observations with SparsePak, as indicated by recent observations[7].

3.5 FRD vs wavelength

We tested all the fibres over the full wavelength range from v through I for an input f-ratio of f/4.2 and found no convincing evidence for wavelength dependence to FRD. Since FRD increases with the input f-ratio, we also obtained filter sequences for the SparsePak Reference fibre for an f/13.7 input beam, but this too showed no sign of variation with wavelength – see Fig. 7.

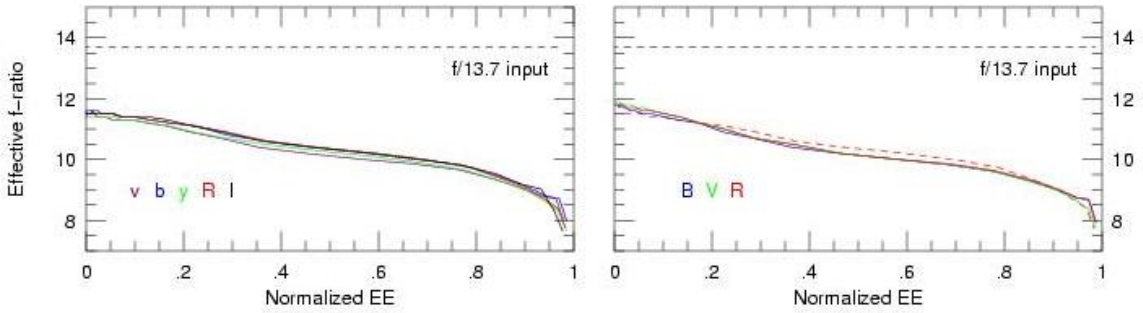

Fig. 7: Effective f-ratio vs normalized EE for the SparsePak Reference fibre with an f/13.7 input beam. On the left is a set of measurements (showing no wavelength dependence) and on the right is the same for BVR bands, obtained after the correction of a significant misalignment in the assembly making up the fibre input mount. The lines are coded for band-pass as given by the coloured labels in the plot. The R-band measurement from the left panel is repeated for reference as a dashed line in the right-hand panel. The two sets are essentially the same, indicating that FRD is not particularly sensitive to such small deviations from telecentricity and hence the quality of our measurements was not badly compromised by the non-telecentric wedge.

3.6 FRD and termination issues

It is well known that poor fibre termination and polishing can lead to both throughput degradation and increased FRD. In preparing our selection of fibres, stainless steel hypodermic tubes with inner diameters close (but slightly over-sized) to the fibre outer diameters were glued into brass ferrules, i.e., cylinders with v-grooves cut down the long-axis for tube seating. In all but one case, the fibres were inserted into the hypodermics and the ends tacked in place with Norland 61 UV curing epoxy. The FBP 600 micron fibre did not fit into the hypodermics and so it was glued directly into the brass ferrules. With the epoxy set, a fibre end could be mounted to the Ultrapol 1200 lapping machine, which uses a series of disks with progressively finer grit for polishing and distilled water for rinsing. The best prepared fibre in our sample is the 500 micron SparsePak Reference cable, which was polished in 2001 using a descending series of grit from 60, 40, 30, 14, 10, 5, 1 and finally 0.5 microns. In contrast, polishing done on newer fibre in 2003 and 2008 was done using a series of 30, 15, 10, 5, and 1 micron grit, other conditions being the same.

Some of our early measurements showed that the FRD was surprisingly bad in the new fibres and visual inspection with a microscope revealed that the increased FRD is likely due to the fibre ends themselves. The most egregious cases had clear fractures in the core. When these were redone, there were substantial improvements in FRD and throughput. For example, one end of the Polymicro FVP 400 was both re-glued and re-polished while the other end was merely re-polished. The fibre beam f-ratios at EE95 increased by between 10 and 20% (measured as the change in the fibre beam f-ratios over the direct beam f-ratio) with the greatest improvement being in the blue, and the throughput increased by approximately 10% across the spectral range – see Fig. 8. The scratch and dig level on the SparsePak Reference Cable

was lower than the other cables, and it indeed performs best. In the future we recommend a calibration of the scratch and dig count vs fibre performance as a reference metric for fibre polishing for astronomical applications.

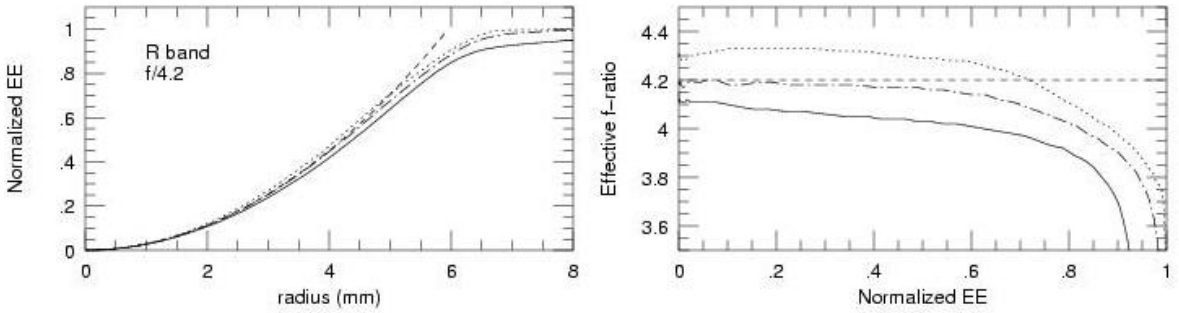

Fig. 8: Demonstration of the significant impact of end-effects on FRD. The 35 m Polymicro FVP 400/440/480 fibre was measured in the R-band for an f/4.2 input beam, first with the termination and polish dating from 2003 (solid line), and then again in 2008 after careful re-termination and re-polishing (dot-dashed line). The SparsePak Reference cable is included for comparison (dotted line), as is the ideal f/4.2 input beam – shown as a dashed line.

3.7 Throughput vs beam-speed

The right-hand panel of Fig. 9 illustrates a subtle (2%) total throughput decrease in the SparsePak Reference fibre as the input beam is slowed down from f/3 to f/14. This is different to, e.g., Ramsey's (1988) throughput vs beam-speed as measured within an aperture equivalent to the input f-ratio, which combines FRD effects in the output beam-speed with losses. The implications are that a larger fraction of the power in slower modes (those propagating more nearly parallel to the fibre optical axis) is scattered into lossy modes. This raises the interesting prospect that fibres fed by fast beams (f/3 to f/4) from telescopes with central obstructions are the most efficient fibre-coupled systems in an absolute sense. Given the small amount of FRD seen at these speeds (e.g., the left panel of Fig. 9), this could open up the efficient use of cost-effective catadioptrics in fibre-fed spectrographs with obstructions well-matched to obstructions in the input beam.

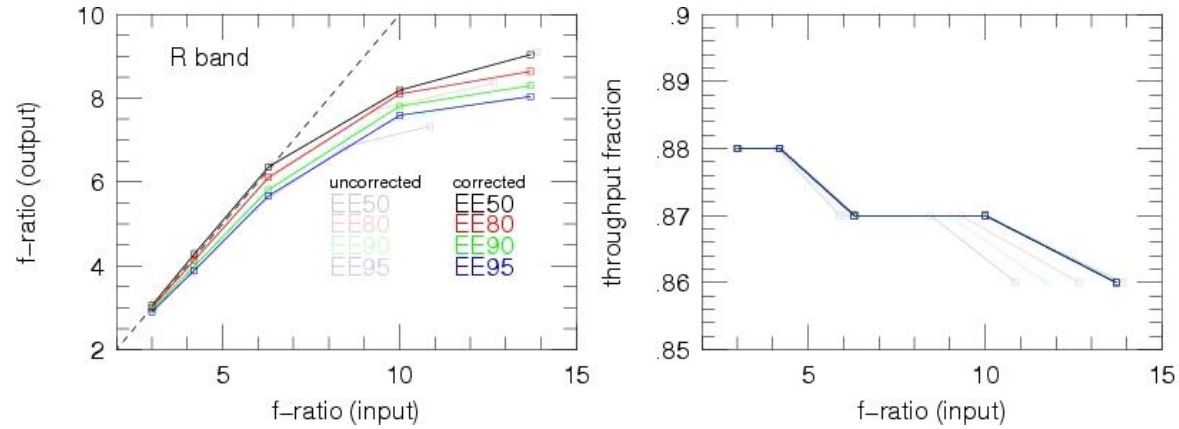

Fig. 9: The effect of FRD is always worse for slow input beams (f-ratio > 5), as seen in the left panel which shows R-band measurements for the SparsePak Reference fibre. Evident in the right-hand panel is a weak trend of throughput decreasing with increasing input f-ratio, indicating that the modes entering near normal to the fibre are the lossiest.

4. DISCUSSION AND SUMMARY

While it is well known that common sources of FRD include poor fibre termination and handling (stress and poor polish) as well as non-telecentricity, it is also widely believed that micro-bending contributes significantly. The latter predicts a wavelength dependence to FRD (Gloge, 1972), with FRD increasing at longer wavelengths. FRD wavelength dependence has been observed by some (Carrasco & Parry 1994, Poppett & Allington-Smith 2007), but not by others (Schmoll et al. 2003, Bershady et al. 2004). Those studies where the effect is seen indicate that the amplitude of the wavelength dependence is far less than predicted by the model. Once possibility is that micro-bending is a rather small, and perhaps inconsequential, contributor to FRD. In the SparsePak reference cable, a large-diameter fibre optic, where there is rather modest levels of FRD (indicating good polish and termination), there is no measurable wavelength dependence from 370 to 880 nm – both at f/4.2 (Fig. 4) and f/13.7 (Fig. 7). It would be interesting to test whether there is any indication that wavelength dependence to FRD increases for smaller-diameter fibres where micro-bending is expected to be more important.

We found the Polymicro FBP fibre has a considerably flatter spectral response than the Polymicro FIP-STU, FVP, or the CeramOptec UV fibre types, making it the best broad-band product on the market. Furthermore, there is no indication that spectral response is dependent on fibre diameter in the 200 – 600 micron range. To our surprise, the SparsePak Reference cable, alleged to be Polymicro FIP fibre, turned out to more closely match the Polymicro FIP-STU transmission curve. This indicates that the SparsePak IFU should in fact perform better than expected down to 400 nm.

Future work will focus on completing the laser injection system for measuring FRD and will also include re-polishing the FBP fibres. Improving their termination will reduce the FRD component introduced by end-effects and after eliminating the last wedge angle in our re-imaging system, we will remeasure the FBP fibres. Those data will ultimately be compared with results to be obtained with the laser injection system.

ACKNOWLEDGMENTS

Research support comes from SAAO, the National Science Foundation (AST-0607516, AST-0804576), and a charitable gift from the Fluno Family to UW-Madison Astronomy. We thank Scott Buckley for design and fabrication of optomechanical components.

REFERENCES

[1] Poppett, C. L., and Allington-Smith, J. R., "Fibre systems for future astronomy: anomalous wavelength-temperature effects," MNRAS, 379, 143 (2007)

[2] Gloge D., Bell. Syst. Tech. J., 151, 1767 (1972)

[3] Carrasco, E. and Parry, I. R., "A method for determining the focal ratio degradation of optical fibres for astronomy," MNRAS, 271, 1 (1994)

[4] Ramsey, L. W., "Focal ratio degradation in optical fibers of astronomical interest," ASPC, 3, 26 (1988)

[5] Bershady, M. A., Andersen, D. R., Harker, J., Ramsey, L. W., Verheijen, M. A. W., "SparsePak: a formatted fiber field-unit for the WIYN Telescope Bench Spectrograph. I. Design, Construction, and Calibration," PASP, 116, 565 (2004)

[6] Bershady, M. A., Andersen, D. R., Verheijen, M. A. W., Westfall, K. B., Crawford, S. M., Swaters, R. A., "SparsePak: a formatted fiber field-unit for the WIYN Telescope Bench Spectrograph. II. On-Sky Performance," ApJS, 156, 311 (2005)

M. Wolf, private communication